Magnetic field induced alignment–orientation conversion: Nonlinear energy shift and predissociation in Te2 B1 u state

M. Auzinsh, A. V. Stolyarov, M. Tamanis, and R. Ferber

Citation: The Journal of Chemical Physics **105**, 37 (1996); doi: 10.1063/1.471833
View online: http://dx.doi.org/10.1063/1.471833
View Table of Contents: http://scitation.aip.org/content/aip/journal/jcp/105/1?ver=pdfcov
Published by the AIP Publishing

Magnetic field induced alignment–orientation conversion: Nonlinear energy shift and predissociation in Te_2 $B1_u$ state

M. Auzinsh, A. V. Stolyarov,[a] M. Tamanis, and R. Ferber
Department of Physics, University of Latvia, Riga, LV-1586, Latvia

(Received 29 December 1995; accepted 28 March 1996)

The paper analyzes magnetic field induced alignment–orientation conversion (AOC) phenomenon caused by simultaneous effect of quadratic terms in Zeeman energy shift and magnetic predissociation (PD), producing asymmetry either in energy splitting $\omega_{MM\pm1}\neq\omega_{-M\mp1-M}$ or in relaxation of coherence $\Gamma_{MM\pm1}\neq\Gamma_{-M\mp1-M}$ between coherently excited M, $M\pm1$ magnetic sublevels. The AOC is registered via the appearance of circular polarization (C) of fluorescence under linearly polarized excitation. The unified perturbation treatment of a molecule in external magnetic field B is presented, accounting for magnetic and intramolecular perturbations via interaction with bonded or continuum states, considering Hund's (c)-case coupling and dividing the intramolecular perturbation operator into homogeneous ($\Delta\Omega=0$) and heterogeneous ($\Delta\Omega=\pm1$) parts. Explicit expressions up to B^2 terms are given for energy shift and PD rate, adapted to 1_u state in conditions relevant to the $B\ ^3\Sigma_u^-$ complex of Te_2 molecule. Numeric simulation revealed that nonlinear magnetic energy shift and heterogeneous magnetic PD produce dispersion type fluorescence circularity signals $C(B)$ of different sign. Fitting of experimental data on $B1_u^-$, $v(J)=2(96)$ state of $^{130}Te_2$ molecule allowed to determine the electronic matrix element of paramagnetic Hamiltonian $(\Omega=0|\hat{\mathbf{H}}_{\rm pm}|\Omega=1)\equiv G_{\pm}=2.7$, as well as the natural $C_v^{\rm het}=\pm6\ {\rm s}^{-1/2}$ and the magnetic $\alpha_v^{\rm het}=\mp9\times10^3\ {\rm s}^{-1/2}\ {\rm T}^{-1}$ rate constants of heterogeneous PD, supposing that the $B1_u^-$ state PD takes place through 0_u^- state continuum. As a result, magnetic AOC represents a sensitive method to investigate molecular structure and intramolecular interaction between both bonded and continuum states. Additionally, it has been shown that the magnetic PD effect leads to strong amplification of nonzero field level crossing signals caused by B^2 terms in Zeeman energy shift.
 [S0021-9606(96)01325-6]

I. INTRODUCTION

The anisotropic spatial distribution of angular momenta in the ensemble of atoms or molecules is characterized in terms of alignment and orientation. One speaks of *alignment* when the distribution is symmetrical with respect to the reflection in the plane which is perpendicular to a certain symmetry axis, and of *orientation* if such symmetry is absent, thus bringing into existence a preferable direction along the symmetry axis. For clarity reason one may imagine that alignment behaves like a double-headed arrow ($\Leftrightarrow$) whereas orientation behaves like a single-headed one ($\Rightarrow$). In particular, excitation with linear polarized light creates alignment only, and $\hat{\mathbf{E}}$-vector defines the axis of cylindrical symmetry. It has been interest for a long time, starting from Refs. 1–3, to study the perturbing factors, which are able to break the reflection symmetry and thus to cause alignment–orientation conversion (AOC). The more recent publications, dealing with different versions of AOC in atoms and molecules, can be found as references given in Ref. 4, to which, for completeness sake, we would like to add the works of Refs. 5–12. The case of AOC in diatomic molecules was investigated in Refs. 4, 8–13. It is easy to understand the main reasons for AOC if one remembers that the ensemble density matrix element $f_{MM'}$ which is obtained as a solution of the stationary density matrix equation of motion and which describes the coherence between sublevels with magnetic quantum numbers M and M' in the state with definite angular momentum J value, contains a factor $(\Gamma_{MM'}+i\omega_{MM'})^{-1}$, namely

$$f_{MM'}\propto\frac{1}{\Gamma_{MM'}+i\omega_{MM'}},\tag{1}$$

where

$$\omega_{MM'}=\frac{E_M-E_{M'}}{\hbar}\tag{2}$$

is the splitting between Zeeman sublevels M,M' with energies $E_M,E_{M'}$, while

$$\Gamma_{MM'}=\frac{\Gamma_M+\Gamma_{M'}}{2}\tag{3}$$

is the rate of relaxation of coherence between M,M' sublevels, Γ_M and $\Gamma_{M'}$ being relaxation rate constants of respective states. It can be seen from the form of Eq. (1) that, generally speaking, at broad spectral line excitation there are two basic reasons for the appearance of AOC in the excited state angular momenta ensemble. Indeed, as it follows from the analysis presented in Ref. 12, one must have such a perturbation which leads to the asymmetry, with respect to the M,M', either in energy splittings

[a]Present address: Department of Chemistry, Moscow State University, 119899, Moscow, Russia.

$$\omega_{MM\pm1} \neq \omega_{-M\mp1-M}, \tag{4}$$

or in M-dependent coherence relaxation rate constants

$$\Gamma_{MM\pm1} \neq \Gamma_{-M\mp1-M}. \tag{5}$$

In a number of our previous publications[4,11–13] the AOC effect in diatomic molecules was treated theoretically and demonstrated experimentally in the case when it has been caused by nonlinear, in particular quadratic Zeeman energy E_M dependence on external static magnetic (**B**) or electric (**E**) field strength, as well as on magnetic quantum numbers M, thus entailing the condition (4). Sufficiently pronounced AOC signal was registered[11] in $B1_u^-$ component of the Te_2 $B\ ^3\Sigma_u^-$ state complex as the appearance of the degree of fluorescence circularity $C(B)$ up to 0.05, under linearly polarized $X1_g^- \rightarrow B1_u^-$ excitation in the presence of static magnetic field up to $B=0.4$ T. The effect has been described as a result of the asymmetric splitting of Zeeman sublevels, see Eq. (4), due to the presence of quadratic Zeeman effect energy shift term. We found it to be a nice example of the magnetic field assisted $\Delta J=\pm1$ mixing of states with different electronic parity, or $e\sim f$ mixing, not only between Ω-doubling components $B1_u^- \sim B1_u^+$ of the electronic $B\ ^3\Sigma_u^-$ state, but rather that of the $B1_u^- \sim B0_u^+$ close together situated components interaction. It is important to stress that both interactions are forbidden in the absence of the external magnetic field. Such a heavy diatomic molecule, without hyperfine structure, as Te_2, possessing well enough investigated energy levels and dynamic parameters (molecular constants, intramolecular interaction parameters, lifetimes, Landé factors, etc.), see Refs. 14 and 15 and references therein, can be considered as one of the ''test'' objects in molecular spectroscopy, along with such diatomics as Na_2, I_2, and others. At the same time, whilst the general behavior of AOC in Te_2 ($B1_u^-$) was well enough described by the treatment developed in Ref. 11, there remained the unexplained additional structure of the experimentally registered signal. To explain such a structure, it needs to be ascertained if there is some influence of another fundamental reason for AOC, namely of the asymmetric over M, $M\pm1$, in the sense of condition (5), relaxation rates $\Gamma_{MM'}$. Indeed, as it was demonstrated in Refs. 8 and 9 on the iodine molecule I_2 in the $B\ ^3\Pi_{0_u^+}$ state, fluorescence circularity may appear owing to magnetic field effected M-selective predissociation (PD). The authors of Refs. 8 and 9 have presented the detailed PD theory,[10] accounting for rotational, magnetic, and hyperfine PD, but they neglected the possible influence of Zeeman effect induced energy shifts in signal description. As it becomes clear even from the first glance at the dense electronic term scheme of Te_2 molecule,[15,16] it is highly probable that such AOC mechanism as the magnetic PD effect, causing the fulfillment of condition (5), has to be taken into account, along with quadratic Zeeman effect terms in energy shift, causing the fulfillment of condition (4).

The main purpose of the present article is to develop an extended treatment of AOC by accounting simultaneously both for quadratic terms in Zeeman effect induced energy shift as well as for magnetic field induced PD. The consideration presented supplies more satisfactory interpretation of experimental results of Ref. 11 on Te_2 $B1_u^-$ state and demonstrates the possibility to determine separately the electronic mixing parameters, to distinguish between homogeneous and heterogeneous PD types and to determine the parameters of very weak natural and magnetic PD.

The paper has a following structure. In Sec. II we will remind briefly the analytical expressions for density matrix elements and fluorescence intensity with a definite, in particular circular polarization, dependent on magnetic field affected $\omega_{MM'}$ and $\Gamma_{MM'}$. In Sec. III a general approach is developed to describe a diatomic molecule in external magnetic field, including both magnetic energy shifts and magnetic PD. A quick description of Te_2 excited electronic states, which are involved in the processes under discussion, is given in Sec. IV. In Sec. V we will pass to the simulations of expected signals in conditions typical for the $B\ ^3\Sigma_u^-$ state of Te_2 molecule, including fluorescence circularity under linear polarized excitation, as well as to the fitting of experimentally obtained data, ending with a summarizing discussion in Sec. VI.

II. FLUORESCENCE INTENSITY

We will discuss the manifestation of AOC in fluorescence signal as the appearance of circular polarization under linear polarized broad spectral line excitation. The detailed treatment is given elsewhere[4,12] and we will stress hereafter the main points only. Let us assume that the weak linearly polarized cw broad spectral light had prepared excited (J') state density matrix $f_{MM'}$.[12,17] The explicit form of intensity expression I_f for light emitted at a $J' \rightarrow J_1''$ transition is

$$I_f(\hat{\mathbf{E}}_\mathbf{f}) = \frac{K|(J_1''\|D\|J')|^2}{2J'+1} \sum_{\mu MM' q_1 q_2} f_{MM'}(-1)^{q_1+q_2} \times (E_f^{-q_1})^* (E_f^{-q_2}) C^{J'M}_{J_1''\mu 1 q_1} C^{J'M'}_{J_1''\mu 1 q_2}, \tag{6}$$

where $E_f^{q_i}$, $q_i=0,\pm1$ are cyclic components of unit fluorescence polarization vector $\hat{\mathbf{E}}_\mathbf{f}$, $C^{J'M}_{J_1''\mu 1 q_1}$ are Clebsch–Gordan coefficients, M, M', and μ are respective excited (J') and ground (J_1'') state magnetic quantum numbers, $(J_1''\|D\|J')$ denotes reduced matrix element for electric dipole transition, K is proportionality factor. The excited state orientation is certified through circularity of fluorescence,

$$C = \frac{I_r - I_l}{I_r + I_l}, \tag{7}$$

$I_{r,l}$ being right-handed and left-handed circularly polarized light intensities. The excited state density matrix elements $f_{MM'}$ are formed in $|J''\mu\rangle \rightarrow |J'M\rangle$ absorption and can be found as stationary solution of the equation of motion[12] as

$$f_{MM'}=\frac{\tilde{\Gamma}_p|(J'\|D\|J'')|^2}{2J'+1}\frac{1}{\Gamma_{MM'}+i\omega_{MM'}}\times\sum_{\mu q_1 q_2}(E^{q_1})^*(E^{q_2})C^{J'M}_{J''\mu 1 q_1}C^{J'M'}_{J''\mu 1 q_2}, \tag{8}$$

where the factor $\tilde{\Gamma}_p|(J'\|D\|J'')|^2/(2J'+1)$ is the dynamic part of absorption probability, E^{q_i} are cyclic components of exciting light vector $\hat{\mathbf{E}}$. Let us assume that the exciting light linear polarization vector $\mathbf{E}(\vartheta,\varphi)$ is directed at angles ϑ,φ with respect to the quantization axis $\mathbf{z}\|\mathbf{B}$, while fluorescence is observed along y axis. These conditions make it possible to find exciting light and fluorescence light vector cyclic components E^{q_i} and $E_f^{q_i}$ by means of Wigner D matrices, thus allowing to write explicitly the expressions for I_r-I_l and I_r+I_l (Refs. 4 and 12) entering Eq. (7). The final expression for the difference I_r-I_l which describes the appearance of orientation can be written as

$$I_r-I_l\propto\Gamma_p\frac{\sin 2\vartheta}{2}\sum_M\frac{\Gamma_{MM+1}\sin\varphi+\omega_{MM+1}\cos\varphi}{\Gamma^2_{MM+1}+\omega^2_{MM+1}}\times(C^{J'M}_{J''M+11-1}C^{J'M+1}_{J''M110}-C^{J'M}_{J''M10}C^{J'M+1}_{J''M11})\times(C^{J'M}_{J''_1M10}C^{J'M+1}_{J''_1M11}+C^{J'M}_{J''_1M+11-1}C^{J'M+1}_{J''_1M+110}). \tag{9}$$

Expression for I_r+I_l takes the form:

$$I_r+I_l\propto\sum_M\left\{\frac{\Gamma_p}{\Gamma_{MM}}\left\{\frac{\sin^2\vartheta}{2}[(C^{J'M}_{J''M-111})^2+(C^{J'M}_{J''M+11-1})^2]+\cos^2\vartheta(C^{J'M}_{J''M10})^2\right\}\left[\frac{1}{2}(C^{J'M}_{J''_1M-111})^2+(C^{J'M}_{J''_1M10})^2+\frac{1}{2}(C^{J'M}_{J''_1M+11-1})^2\right]+\Gamma_p\frac{\sin^2\vartheta}{2}\frac{\Gamma_{M-1M+1}\cos 2\varphi-\omega_{M-1M+1}\sin 2\varphi}{\Gamma^2_{M-1M+1}+\omega^2_{M-1M+1}}\times C^{J'M-1}_{J''M1-1}C^{J'M+1}_{J''M11}C^{J'M-1}_{J''_1M1-1}C^{J'M+1}_{J''_1M11}\right\}. \tag{10}$$

Consequently, as it follows clearly from Eqs. (9) and (10), in order to analyze the appearance of magnetic field induced orientation, one has to calculate:

(i) the magnetic field induced energy splitting $\omega_{MM'}$ values, which are defined by the magnetic sublevel energy set $E_M(B)$, see Eq. (2);

(ii) the magnetic field affected coherence relaxation constant values $\Gamma_{MM'}$ between M,M' sublevels, which are defined by the magnetic field-dependent relaxation constant set $\Gamma_M(B)$, see Eq. (3).

For this purpose we will further consider the Zeeman effect induced energy shifts to account for (i), as well as the magnetic predissociation to account for (ii).

III. LINEAR AND QUADRATIC TERMS IN ZEEMAN SHIFT AND MAGNETIC PREDISSOCIATION

The Hamiltonian $\hat{\mathbf{H}}$ of a molecule in external stationary homogeneous magnetic field $\mathbf{B}$ can be presented in a simplified form as[18]

$$\hat{\mathbf{H}}=\hat{\mathbf{H}}_\mathbf{0}+\hat{\mathbf{V}}+\hat{\mathbf{H}}_\mathbf{pm}+\hat{\mathbf{H}}_\mathbf{dm}, \tag{11}$$

where $\hat{\mathbf{H}}_\mathbf{0}+\hat{\mathbf{V}}$ is the Hamiltonian of an isolated molecule without external field, $\hat{\mathbf{H}}_\mathbf{0}$ is the Hamiltonian zero approximation, $\hat{\mathbf{V}}$ is the perturbation operator of intramolecular interactions,

$$\hat{\mathbf{H}}_\mathbf{pm}=-\mu_B\mathbf{B}(g_l\mathbf{J_a}+(g_s-g_l)\mathbf{S}) \tag{12}$$

is the so-called paramagnetic term, μ_B is Bohr magneton, g_l and g_s are orbital and spin electronic g factors, respectively ($g_l=-1$ and $g_s=-2$), $\mathbf{J_a}=\mathbf{L}+\mathbf{S}$ is the total electronic angular momentum

$$\hat{\mathbf{H}}_\mathbf{dm}=K_\mathbf{dm}\sum_i[\mathbf{B}\times\mathbf{r_i}]^2 \tag{13}$$

is the so-called diamagnetic term, i denoting summation over all electrons, $K_{\rm dm}=e^2/8m_ec^2=\mu_B^2m_e/2\hbar^2\simeq 2.2\times10^{-4}\mu_B^2$ (in atomic units). In Eqs. (11)–(13) we have neglected the nuclear spins and the relativistic effects leading to quantumelectrodynamical correction to g_l and g_s values.

We will further consider that $\hat{\mathbf{V}}$, $\hat{\mathbf{H}}_{\rm pm}$, and $\hat{\mathbf{H}}_{\rm dm}$ are small in comparison with $\hat{\mathbf{H}}_\mathbf{0}$, which allows one to use first- and second-order nondegenerative perturbation theory to describe the Zeeman effect induced energy shifts as well as the intramolecular interaction effects. We will use Fermi–Wentzel golden rule do describe natural and magnetic PD.[19] In further consideration we will account for magnetic field and intramolecular perturbation influence on the eigenfunctions, but neglect the level shifts caused by PD. Then, since we are interested mainly in $\omega_{MM'}$ and $\Gamma_{MM'}$ dependencies on magnetic quantum numbers M and magnetic field strength B, and restricting our consideration up to terms containing B^2, we have to pass from Eqs. (11)–(13) to the following expressions for level energy E_M and predissociation rate Γ_M:

$$E_M^{\Phi J}=E_{\rm nat}^{\Phi J}+\langle\Phi_pJM|\hat{\mathbf{H}}_\mathbf{pm}|\Phi_pJM\rangle+\sum_{\Phi'_pJ'}\frac{|\langle\Phi_pJM|\hat{\mathbf{H}}_\mathbf{pm}|\Phi'_pJ'M\rangle|^2}{E_M^{\Phi_pJ}-E_M^{\Phi'_pJ'}}+\langle\Phi_pJM|\hat{\mathbf{H}}_\mathbf{dm}|\Phi_pJM\rangle, \tag{14}$$

$$\Gamma_M^{\Phi J}=\Gamma_{\rm nat}^{\Phi J}+\frac{2\pi}{\hbar}\left[\sum_{\Phi'J'}\left|\langle\Phi JM|\hat{\mathbf{H}}_\mathbf{pm}|\Phi'J'M\rangle\right|^2+2\sum_{\Phi'}\langle\Phi JM|\hat{\mathbf{V}}|\Phi'JM\rangle\langle\Phi JM|\hat{\mathbf{H}}_\mathbf{pm}+\hat{\mathbf{H}}_\mathbf{dm}|\Phi'JM\rangle\right], \tag{15}$$

where $E_{\rm nat}^{\Phi J}$ and $\Gamma_{\rm nat}^{\Phi J}$ are respective energy shift and predissociation rate values for a certain rovibrational level in ab-

sence of external field, $|\Phi JM\rangle$ are eigenfunctions of the $\hat{\mathbf{H}}_\mathbf{0}$ Hamiltonian, while $E_M^{\Phi_p J}$ and $|\Phi_p J'M\rangle$ are eigenvalues and eigenfunctions of the $\hat{\mathbf{H}}_\mathbf{0}+\hat{\mathbf{V}}$ Hamiltonian. For the reason which will be clear from the following discussion, the diamagnetic perturbation has been taken into account only to the first order perturbation theory in Eq. (14). Functions $|\Phi'_p J'M\rangle$ or $|\Phi' JM\rangle$ may correspond either to bonded [Eq. (14)] or to continuum [Eq. (15)] states, with which intramolecular interaction is taking place. It is supposed that $|\Phi' JM\rangle$ in Eq. (15) are the energy-normalized continuum wave functions. Summands containing $\hat{\mathbf{H}}_{\rm pm}$ in Eq. (14) are the first- and second-order perturbation terms, respectively, the second-order term being the so-called ''high-frequency term'' according to Van Vleck.[20] Now we can write the eigenfunctions $|\Phi_p^{(B)} JM\rangle$ which are perturbed by magnetic field

$$|\Phi_p^{(B)} JM\rangle = |\Phi_p JM\rangle + \sum_{\Phi'_p J'} \frac{\langle \Phi_p JM|\hat{\mathbf{H}}_{\mathbf{pm}}|\Phi'_p J'M\rangle}{E_M^{\Phi_p J} - E_M^{\Phi'_p J'}} |\Phi'_p J'M\rangle, \tag{16}$$

where the symbol $|\Phi_p JM\rangle$ denotes state wave function in the absence of magnetic field, but with accounting for intramolecular perturbations, namely

$$|\Phi_p JM\rangle = |\Phi JM\rangle + \sum_{\Phi'} \frac{\langle \Phi JM|\hat{\mathbf{V}}|\Phi' JM\rangle}{E_J^{\Phi} - E_J^{\Phi'}} |\Phi' JM\rangle. \tag{17}$$

Matrix elements of the $\hat{\mathbf{H}}_\mathbf{0}+\hat{\mathbf{V}}$ operator are independent of magnetic quantum number M, whereas $\hat{\mathbf{H}}_{\rm pm}$ and $\hat{\mathbf{H}}_{\rm dm}$ dependence on M is given by Wigner–Eckart theorem in laboratory coordinates[21,22]

$$\langle J'M'|\hat{f}_0^{(k)}|JM\rangle = (-1)^{J'-M'} \begin{pmatrix} J' & kJ \\ -M' & 0M \end{pmatrix} \times \langle J'\|\hat{f}^{(k)}\|J\rangle, \tag{18}$$

where $\hat{f}_0^{(k)}$ denotes operator spherical tensorial components of rank k and projection $q=0$, $\langle J'\|f^{(k)}\|J\rangle$ are reduced matrix elements, $\left(\begin{smallmatrix} J' & kJ \\ -M' & 0M \end{smallmatrix}\right)$ are $3j$ symbols used here because of their higher symmetry instead of Clebsch–Gordan coefficients. Let us remind that the spherical functions Y_{k0} of rank $k=0,1,2$, being a particular type of the spherical tensor, have the following dependence on the spherical angle ϑ': $Y_{00}=\text{const}$, $Y_{10}\propto\cos\vartheta'$ and $Y_{20}\propto(3\cos^2\vartheta'-1)$. As follows from Eq. (12), $\hat{\mathbf{H}}_{\rm pm}$ is defined as the scalar product of two vectors, thus $\hat{\mathbf{H}}_{\rm pm}$ contains $\cos\vartheta'$ and corresponds to the first rank ($k=1$) tensor. At the same time, $\hat{\mathbf{H}}_{\rm dm}$ contains $\sin^2\vartheta'$, see Eq. (13), and thus corresponds to zero ($k=0$) and second ($k=2$) rank tensors. Hence, the respective selection rules over J are: $\Delta J=0,\pm1$ for $\hat{\mathbf{H}}_{\rm pm}$ and $\Delta J=0,\pm1,\pm2$ for $\hat{\mathbf{H}}_{\rm dm}$. Remember that, for the case of intramolecular interaction, the selection rule over J is $\Delta J=0$ only. Besides, the additional symmetry selection rules for both magnetic and intramolecular interactions are $\oplus\leftrightarrow\ominus$ with respect to the full parity and, additionally, $s\leftrightarrow a$ regarding symmetric/antisymmetric states in the case of a homonuclear diatomic molecule (see Fig. 2). In order such requirements to be obeyed, only the $3j$ symbols with $\Delta J=J'-J=0,\pm1,\pm2$ and with $M'=M$ have to be considered. The explicit expressions for $3j$ symbols are given in Table I. In particular, as follows from the table, the diagonal terms of Hamiltonian $\hat{\mathbf{H}}_{\rm pm}^{(1)}$ are linear over M. The diagonal ($J'=J$) Hamiltonian matrix elements are M independent for $\hat{\mathbf{H}}_{\rm dm}^{(0)}$, while for $\hat{\mathbf{H}}_{\rm dm}^{(2)}$ they contain the factor $[3M^2-J(J+1)]$. The squared nondiagonal Hamiltonian matrix elements ($J-J'=\pm1$) contain the factor $(J+1)^2-M^2$ for $\hat{\mathbf{H}}_{\rm pm}^{(1)}$. These considerations allow one to obtain from Eqs. (14)–(15) the general dependence of E_M and Γ_M on M and B in closed form as

$$E_M = a + bMB + (c + dM^2)B^2, \tag{19}$$

$$\Gamma_M = a' + b'MB + (c' + d'M^2)B^2, \tag{20}$$

where parameters a,b,c,d the and a',b',c',d' are independent of M and B, being dependent on other quantum numbers characterizing isolated molecules in the absence of external field. From Eqs. (19)–(20) one may judge immediately that the conditions described by Eqs. (4)–(5) are fulfilled.

Further, since $\hat{\mathbf{V}}$ and $\hat{\mathbf{H}}_{\rm pm}$ are composed from angular momenta **J**, **L**, and **S**, the evaluation of $a-d$ and $a'-d'$ parameters in Eqs. (19)–(20) will depend on the particular type of the angular momenta coupling. We will consider here the primitive Hund's (c)-case coupling scheme,[19] according to which the full rovibrational Hamiltonian can be split into parts in the following way. The zero-order Hamiltonian $\hat{\mathbf{H}}_\mathbf{0}$, see Eq. (11), includes:

(i) *electronic* term $\hat{\mathbf{H}}_{\rm el}^{\mathbf{0}}(R,\mathbf{r_i})$ which, however, contains all relativistic effects caused by spin–orbit and spin–spin interactions;

(ii) *vibrational* term in form $-(1/2\mu)(\partial^2/\partial R^2)$, where μ is reduced mass of the molecule, R is internuclear distance;

(iii) *rotational* term in form $B(R)\mathbf{J^2}$, with eigenvalues $\hbar^2 B(R)J(J+1)$, where $B(R)=1/(2\mu R^2)$.

In doing so, we will also consider that for the eigenfunctions $|\Psi_\Omega(R,\mathbf{r_i})\rangle$ of Hamiltonian $\hat{\mathbf{H}}_{\rm el}^{\mathbf{0}}(R,\mathbf{r_i})$, which are obtained via solving the equation $\hat{\mathbf{H}}_{\rm el}^{\mathbf{0}}(R,\mathbf{r_i})\Psi_\Omega(R,\mathbf{r_i}) = E_{\rm el}^{\Omega}(R)\Psi_\Omega(R,\mathbf{r_i})$, the relations $\langle\Psi_\Omega|\partial\Psi_{\Omega'}/\partial R\rangle \equiv\langle\Psi_\Omega|\partial^2\Psi_{\Omega'}/\partial R^2\rangle\equiv0$ are fulfilled, Ω denoting J projection on internuclear axis. Such a choice of electronic Hamiltonian corresponds to the so-called diabatic approximation. Thus, in the coupling case under consideration, each Ω component of an (a)-case multiplet is regarded as a separate electronic state with its own potential curve $E^{\Omega}(R)$, the different curves, however, being allowed to intersect each other. According to the described representation of zero-order Hamiltonian $\hat{\mathbf{H}}_\mathbf{0}$, the perturbation operator $\hat{\mathbf{V}}$, which enters Eq. (11), is equal to

TABLE I. $3j$-symbols $\begin{pmatrix} J & k & J' \\ M & l & M' \end{pmatrix} = \begin{pmatrix} J' & k & J \\ -M' & -l & -M \end{pmatrix}$.

$\begin{pmatrix} J0J \\ -M0M \end{pmatrix}$	$(-1)^{J-M}\frac{1}{\sqrt{2J+1}}$
$\begin{pmatrix} J1J \\ -M0M \end{pmatrix}$	$\frac{(1-)^{J-M}M}{\sqrt{J(J+1)(2J+1)}}$
$\begin{pmatrix} J1J \\ -M-11M \end{pmatrix}$	$(1-)^{J-M}\sqrt{\frac{(J-M)(J+M+1)}{(J+1)(2J+1)2J}}$
$\begin{pmatrix} J1J+1 \\ -M0M \end{pmatrix}$	$(-1)^{J-M-1}\sqrt{\frac{(J+1)^2-M^2}{(2J+3)(J+1)(2J+1)}}$
$\begin{pmatrix} J1J+1 \\ -M-11M \end{pmatrix}$	$(-1)^{J-M-1}\sqrt{\frac{(J-M)(J-M+1)}{(2J+3)(2J+2)(2J+1)}}$
$\begin{pmatrix} J2J \\ -M0M \end{pmatrix}$	$\frac{(-1)^{J-M}[3M^2-J(J+1)]}{\sqrt{(2J+3)(J+1)(2J+1)J(2J-1)}}$
$\begin{pmatrix} J2J \\ -M-11M \end{pmatrix}$	$(-1)^{J-M}(2M+1)\sqrt{\frac{6(J+M+1)(J-M)}{(2J+3)(2J+2)(2J+1)2J(2J-1)}}$
$\begin{pmatrix} J2J+1 \\ -M0M \end{pmatrix}$	$(-1)^{J-M+1}M\sqrt{\frac{3[(J+1)^2-M^2]}{(J+2)(2J+3)(J+1)(2J+1)J}}$
$\begin{pmatrix} J2J+1 \\ -M-11M \end{pmatrix}$	$(-1)^{J-M+1}2(J+2M+2)\sqrt{\frac{(J-M+1)(J-M)}{(2J+4)(2J+3)(2J+2)(2J+1)2J}}$
$\begin{pmatrix} J2J+2 \\ -M0M \end{pmatrix}$	$(-1)^{J-M}M\sqrt{\frac{6[(J+2)^2-M^2][(J+1)^2-M^2]}{(2J+5)(2J+4)(2J+3)(2J+2)(2J+1)}}$
$\begin{pmatrix} J2J+2 \\ -M-11M \end{pmatrix}$	$2(-1)^{J-M}\sqrt{\frac{(J+M+2)(J-M+2)(J-M+1)(J-M)}{(2J+5)(2J+4)(2J+3)(2J+2)(2J+1)}}$

$$\hat{\mathbf{V}}=\hat{\mathbf{V}}_{\mathbf{el}}(R,\mathbf{r_i})+B(R)\mathbf{J_a^2}-2B(R)\mathbf{J}\mathbf{J_a}\equiv\hat{\mathbf{V}}_{\mathbf{hom}}+\hat{\mathbf{V}}_{\mathbf{het}}, \quad (21)$$

where $\hat{\mathbf{V}}_{\mathrm{el}}(R,\mathbf{r_i})$ is the part of full electronic Hamiltonian which is not included into $\hat{\mathbf{H}}^{\mathbf{0}}_{\mathrm{el}}(R,\mathbf{r_i})$, while the remaining terms appear from the rotational part of Hamiltonian due to the fact that pure rotational momentum $\mathbf{N}$ is constructed from $\mathbf{J}$ and $\mathbf{J_a}$ as $\mathbf{N}=\mathbf{J}-\mathbf{J_a}$. First and second terms in Eq. (21) do not depend on J explicitly and, consequently, the matrix elements of these operators follow selection rule $\Delta\Omega=0$, thus defining the homogeneous interaction $\hat{\mathbf{V}}_{\mathrm{hom}}$. The third term in Eq. (21) is linearly dependent on J and, hence, obeys the $\Delta\Omega=\pm1$ selection rule. As a result, according to selection rules over Ω, the intramolecular perturbation operator $\hat{\mathbf{V}}$ is divided into respective *homogeneous* $\hat{\mathbf{V}}_{\mathrm{hom}}$ ($\Delta\Omega=0$) and *heterogeneous* $\hat{\mathbf{V}}_{\mathrm{het}}$ ($\Delta\Omega=\pm1$) parts.

The symmetrized basis eigenfunctions $|\Phi JM\rangle$ corresponding to the coupling case under consideration are:

$$|\Phi JM\rangle=\frac{|\Psi_\Omega\rangle}{\sqrt{2}}|v_J\rangle[|\Omega JM\rangle\pm|-\Omega JM\rangle], \quad (22)$$

and for the special case $\Omega=0$:

$$|\Phi JM\rangle=|\Psi_\Omega\rangle|v_J\rangle|\Omega JM\rangle. \quad (23)$$

The vibrational eigenfunction $|v_J\rangle$ is obtained via solution of the radial Schrödinger equation with corresponding effective internuclear potential $U_J^\Omega(R)$:

$$-\frac{1}{2\mu}\frac{d^2|v_J\rangle}{dR^2}+[U_J^\Omega(R)-E_{vJ}^\Omega]|v_J\rangle=0, \quad (24)$$

where $U_J^\Omega(R)=E_{\mathrm{el}}^\Omega(R)+J(J+1)/2\mu R^2$ is an eigenvalue of the $\hat{\mathbf{H}}^{\mathbf{0}}_{\mathrm{el}}(R,\mathbf{r_i})+B(R)\mathbf{J^2}$ operator.

Then, rovibronic matrix elements of homogeneous ($\Delta\Omega=0$) and heterogeneous ($\Delta\Omega=1$) intramolecular interaction, see Eq. (21), which correspond to the chosen basis [see Eq. (22)], can be written as

$$\langle v_J^{\Omega'}|\hat{\mathbf{V}}^{\mathbf{\Omega\Omega'}}_{\mathbf{hom}}(R)|v_J^\Omega\rangle, \quad (25)$$

for $\Omega'=\Omega$, and as

$$-\left\langle v_J^{\Omega'}\left|\frac{\eta_{\mathrm{het}}^{\Omega\Omega'}(R)}{2\mu R^2}\right|v_J^\Omega\right\rangle\sqrt{J(J+1)-|\Omega|(|\Omega|\pm1)} \quad (26)$$

for $\Omega'=\Omega\pm1$, where

$$\eta_{\mathrm{het}}^{\Omega\Omega'}(R)=\langle\Omega'|\hat{\mathbf{J}}_{\mathbf{a}\pm}|\Omega\rangle. \quad (27)$$

To obtain $\hat{\mathbf{H}}_{\mathrm{pm}}$ and $\hat{\mathbf{H}}_{\mathrm{dm}}$ operators dependence on Ω and J quantum numbers, we apply again Wigner–Eckart theorem, now in molecule fixed frame, in order to evaluate the reduced matrix elements which enter Eq. (18):

$$\langle J'\Omega'||\hat{f}^{(k)}||J\Omega\rangle \sim \begin{pmatrix} J' & kJ \\ -\Omega' & l\Omega \end{pmatrix} \langle \Omega'|\hat{f}_l^{(k)}|\Omega\rangle. \tag{28}$$

Considering $\hat{\mathbf{H}}_{\rm pm}^{(1)}$ with $k=1$, $l=\Delta\Omega=0,\pm1$, and $\hat{\mathbf{H}}_{\rm dm}^{(2)}$ with $k=2$, $l=\Delta\Omega=0,\pm1,\pm2$, we can get the following expressions for corresponding electronic matrix elements $\langle\Omega'|\hat{f}_l^{(k)}|\Omega\rangle$:

$$\Omega'=\Omega:\ \langle\Omega|\hat{\mathbf{H}}_{\mathbf{pm}}^{(1)}|\Omega'\rangle = g_l\Omega\,\delta_{\Omega\Omega'}+(g_s-g_l)\langle\Omega|\hat{\mathbf{S}}_{\mathbf{z}}|\Omega'\rangle \equiv G_z(R), \tag{29}$$

$$\Omega'=\Omega\pm1:\ \langle\Omega|\hat{\mathbf{H}}_{\mathbf{pm}}^{(1)}|\Omega'\rangle = g_l\langle\Omega|\hat{\mathbf{J}}_{\mathbf{a}\pm}|\Omega'\rangle+(g_s-g_l)\langle\Omega|\hat{\mathbf{S}}_{\pm}|\Omega'\rangle \equiv G_{\pm}(R), \tag{30}$$

$$\Omega'=\Omega:\begin{cases}\langle\Omega|\hat{\mathbf{H}}_{\mathbf{dm}}^{(0)}|\Omega'\rangle=\dfrac{2}{3}\left\langle\Omega\left|\sum_i \mathbf{r}_\mathbf{i}^2\right|\Omega'\right\rangle\equiv h_{00}(R),\\ \langle\Omega|\hat{\mathbf{H}}_{\mathbf{dm}}^{(2)}|\Omega'\rangle=\left\langle\Omega\left|\sum_i\left(\dfrac{\mathbf{r}_\mathbf{i}^2}{3}-z_i^2\right)\right|\Omega'\right\rangle\equiv h_{20}(R),\end{cases} \tag{31}$$

$$\Omega'=\Omega\pm1:\ \langle\Omega|\hat{\mathbf{H}}_{\mathbf{dm}}^{(2)}|\Omega'\rangle = \left\langle\Omega\left|\sum_i (x_i\pm iy_i)z_i\right|\Omega'\right\rangle\equiv h_{21}(R), \tag{32}$$

$$\Omega'=\Omega\pm2:\ \langle\Omega|\hat{\mathbf{H}}_{\rm dm}^{(2)}|\Omega'\rangle = \left\langle\Omega\left|\sum_i (x_i\pm iy_i)^2\right|\Omega'\right\rangle\equiv h_{22}(R), \tag{33}$$

where $\mathbf{r_i}=\{x_i,y_i,z_i\}$. Using Eqs. (24)–(30) we arrive at following conclusions, which are important for our further discussion:

(1) Homogeneous intramolecular perturbations ($\Delta\Omega=0$) are independent of J whereas the heterogeneous ones increase with J approximately as $[J(J+1)]^{1/2}$, see Eqs. (25), (26);
(2) Homogeneous ($\Delta\Omega=0$) magnetic interaction, caused by $\hat{\mathbf{H}}_{\rm pm}$ operator, decreases with J as $[J(J+1)]^{-1}$, whereas the heterogeneous ones decrease as $[J(J+1)]^{-1/2}$;
(3) Homogeneous mixing, caused by $\hat{\mathbf{H}}_{\rm pm}$ operator, appears only due to $\langle\Omega|\hat{\mathbf{S}}_{\mathbf{z}}|\Omega'\rangle$ term, which is small at least for small internuclear distances since at pure Hund's (a)-case coupling, when $\hat{\mathbf{S}}_{\mathbf{z}}$ is a good quantum number, this mixing is absent at all for $\Omega=\Omega'$ belonging to the different electronic states;
(4) Electronic matrix element $\eta(R)$ of the heterogeneous interaction, see Eq. (27), is a part of electronic matrix element of the paramagnetic term $G_{\pm}(R)$, see Eq. (30).

Proceeding from conclusions (1)–(3), one can expect that, for large J values, the heterogeneous interaction, both intramolecular and magnetic, will be more pronounced than the homogeneous one. To simplify our further treatment, we will assume that:

(i) all electronic matrix elements, corresponding to $\hat{\mathbf{V}}$, $\hat{\mathbf{H}}_{\rm pm}$, and $\hat{\mathbf{H}}_{\rm dm}$ operators, are independent of internuclear distance R;
(ii) vibrational wavefunctions belonging to the same vibronic state are coinciding for adjacent J values, namely
$$|v_i^{J+1}\rangle\cong|v_i^J\rangle\cong|v_i^{J-1}\rangle. \tag{34}$$

In particular, the above assumptions (i) and (ii) lead to the following relation: $\langle v_i|\hat{\mathbf{G}}_{\mathbf{z}}(R)|v_j\rangle = G_z\delta_{v_iv_j}$, where v_i, v_j belong to the same electronic state.

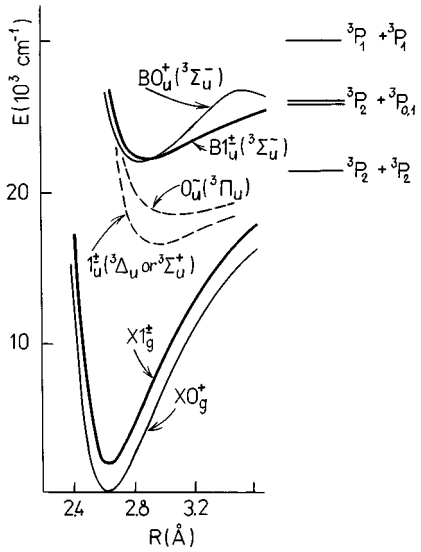

FIG. 1. The pattern of some Te_2 electronic states involved into consideration.

IV. TE_2 TERM PATTERN

Before passing to signal simulation, it is necessary to concentrate briefly onto main features of electronic structure of the molecule under investigation (the even Te_2 isotope will be beard in mind). The detailed inspection of $B\,^3\Sigma_u^-$ terms of Te_2 molecule is presented in our recent paper,[15] see also references therein. We will further keep ourselves to the term structure as proposed in Ref. 15, that is supposing that the closely located bonded $B0_u^+$ and $B1_u^\pm$ states, see Fig. 1, belong basically to the $B\,^3\Sigma_u^-$ state complex. It is necessary to consider the interaction of $B1_u^+\sim B0_u^+$ states caused by electron-rotation interaction. The matrix element $h_{\rm het}^{\Omega\Omega'}$ [see Eq. (27)] of such heterogeneous interaction was determined as $\eta\cong1.35$ from unified self-consistent treatment of energetic, magnetic and radiative measurement data.[15]

It is important to mention that $B1_u^\pm$ state PD in Te_2 molecule was observed directly as a diminution of spontaneous lifetime with v growing for v_i from 2 up to 8 and J from 52 up to 181, see Table II. Note that all these $B1_u^\pm$ state

TABLE II. Experimentally measured (τ_{sp}^{exp}) and theoretically estimated (τ_{sp}^{est}) spontaneous lifetimes of $v(J)$ levels of 1_u^- and 1_u^+ components of $B\,^3\Sigma_u^-$ state of $^{130}Te_2$.

Term	v	J	τ_{sp}^{exp} (ns)	τ_{sp}^{est} (ns)
	2	86	107 (7)	109
	2	96	117(11)	120
1_u^-	4	52	49 (4)	112
	8	70	10 (2)	121
	4	111	66 (5)	115
1_u^+	5	131	45 (6)	120
	8	181	14 (2)	133

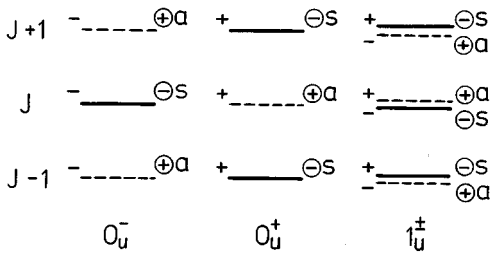

FIG. 2. Symmetry of rovibronic states of Te_2 molecule. The even tellurium isotope and even J value are considered. Dashed lines denote the forbidden states. Symbols $+/-$, or e/f in different notation, refer to electronic parity, symbols $\oplus/\ominus$ refer to full parity, s/a refer to symmetric/antisymmetric states.

levels are situated below the $^3P_2+^3P_{0,1}$ dissociation limit (ca. 26 000 cm^{-1}), which means that the state responsible for PD must approach $^3P_2+^3P_2$ ground electronic state limit. It has been supposed that PD of the $B1_u^\pm$ state levels belongs to the so-called c^- classification type after Mulliken,[23] emerging through a repulsive part of bonded 1_u and/or 0_u states, see Fig. 1. This mechanism follows, in particular, from the weakness of PD while speaking of the $v=2$, $J=96$ level of 1_u^- component of the $B\,^3\Sigma_u^-$ state, which can be proved, in particular, by the existing experimental lifetime data given in Table II. The experiments were performed by laser-induced fluorescence method, using $(v''=4,\ J''=95)X1_g^-\rightarrow(v'=2,\ J'=96)B1_u^-$ absorption of 514.5 Ar^+-laser line.[11,15] The estimated[15] value of spontaneous lifetime τ_{sp} is ca. 110–130 ns.

All possible electronic states approaching $^3P_2+^3P_2$ dissociation limit in (c)-Hund's coupling case are: $0_g^+(3),0_u^-(2),1_g(2),1_u(2),2_g(2),2_u,3_g,3_u,4_u$.[24] Hence, due to the $\Delta\Omega=0,\pm1$, $u\leftrightarrow g$ selection rules for intramolecular interaction, only states 2_u^-, $0_u^-(2)$ or $1_u^-(2)$ approaching $^3P_2+^3P_2$ limit may be responsible for natural heterogeneous or homogeneous very weak $B1_u^-$ state PD. It is worth to mention that, as distinct from the well investigated $B\,^3\Sigma_u^-$ complex, no one of the above discussed electronic states, which could be responsible for natural PD of the $B1_u^-$ state, had been observed in spectroscopic measurements, and the reliable information on molecular constants and potential curves does not exist for them. The only existing publication[16] deals with relativistic *ab initio* evaluation of low lying electronic terms of Te_2 molecule. Unfortunately, the paper[16] does not contain spin–orbit and spin–spin splitting parameters of $^3\Sigma_u^+$, $^3\Pi_u$, and $^3\Delta_u$ terms, the Ω components under discussion are most likely originating from. Therefore we were forced to perform crude estimations of relative location of these components by using the semiempirical scheme described in Ref. 19, which is based on the knowledge of leading electronic configuration of $^3\Sigma_u^+$, $^3\Pi_u$, and $^3\Delta_u$ states, as well as on the empirical spin–orbit constants of separated atoms, which the above molecular terms are converging to at $R\rightarrow\infty$. This allowed us to conclude that the electronic states responsible for $B1_u^-$ state PD, which are most preferable from energy consideration, are the 0_u^- component originating from the $^3\Pi_u$ state and the $1_u^\pm$ components originating from $^3\Sigma_u^+$ or/and $^3\Delta_u$ states, see Fig. 1. We therefore will restrict ourselves with taking into account in PD treatment $B1_u^-\sim0_u^-$ and $B1_u^-\sim1_u^\pm$ interactions only. Since 0_u^- term originates from $^3\Pi_u$, while, $1_u^\pm$ term originates from $^3\Sigma_u^+$ or $^3\Delta_u$, we are able to evaluate the order of magnitude of Franck–Condon factors density (FCD) entering expressions for PD rate, see Sec. V.

The symmetry of rovibronic levels of even isotope Te_2 molecule can be understood from Fig. 2, where J is considered to be an even number. Symbols $+$ or $-$, which correspond to e or f notation respectively, stand for electronic parity, while circled signs $\oplus$ or $\ominus$ refer to total parity. Since nuclear spin is zero, all antisymmetric (a) levels disappear.

V. SIGNAL SIMULATION AND DATA PROCESSING

Now we are going to use the theory presented in Secs. II and III in order to simulate fluorescence signals of different polarization, see Eq. (6), including the appearance of fluorescence circularity, see Eq. (9), for the conditions which are relevant to Te_2 molecule $B1_{u-}\rightarrow X1_g^-$ fluorescence (see Sec. IV) in external magnetic field.

A. Zeeman energy shift, or $\omega_{MM'}$ contribution

Let us first adapt the theory developed in Sec. III to describe the magnetic field dependence of fluorescence polarization and circularity caused by different-order terms in Zeeman effect induced energy shift E_M, see Eq. (14), as appropriate for Te_2 $B1_u^-$ state. Applying Wigner–Eckart theorem, first in laboratory coordinate system, see Eq. (18), and after that in molecular coordinate system, see Eq. (28), accounting for explicit $3j$-symbols formulas (Table I) and implementing vibrational and electronic parts of matrix elements defined by Eqs. (25), (26) and (29)–(33), we arrive at the following energy E_M expressions for the linear paramagnetic term (LPT) and for the high-frequency term (HFT):

$$E_{\mathrm{LPT}}(M,B)=\langle\Phi_pJM|\hat{\mathbf{H}}_{\mathbf{pm}}|\Phi_pJM\rangle=-\frac{\mu_BBMG_z}{J(J+1)},\qquad(35)$$

$$E_{\mathrm{HFT}}(M,B)=\sum_{\Phi'_pJ'}\frac{|\langle\Phi_pJM|\hat{\mathbf{H}}_{\mathbf{pm}}|\Phi'_pJ'M\rangle|^2}{E_M^{\Phi J}-E_M^{\Phi' J'}}=\frac{\mu_B^2B^2}{2}\left\{\frac{G_z^2}{B_v}\left[\frac{(J^2-1)T(J,M)(1+\eta G_{\pm}JS_0/G_z)^2}{J^3}\right.\right.$$
$$\left.-\frac{((J+1)^2-1)T(J+1,M)(1-\eta G_{\pm}(J+1)S_0/G_z)^2}{(J+1)^3}\right]+\frac{G_{\pm}^2}{B_v}\left[\frac{JT(J+1,M)}{J+1}\left(S_1-\frac{2G_z\eta S_3}{G_{\pm}(J+1)}\right)\right.$$
$$\left.\left.+\frac{(J+1)T(J,M)}{J}\left(S_2+\frac{2G_z\eta S_4}{G_{\pm}J}\right)\right]\right\}=E_{\mathrm{HFT}}^0+E_{\mathrm{HFT}}^{\mathrm{int}},\tag{36}$$

where $E_{\mathrm{HFT}}^{\mathrm{int}}$ contains the summands proportional to $G_{\pm}G_z$, whereas E_{HFT}^0 coincides with the previous treatment,[11] which was accomplished without accounting for wave function mixing caused by intramolecular perturbation operator η_{het}, see Eq. (26). The $T(J,M)$ and S_i have the following meaning:

$$T(J,M)=\frac{J^2-M^2}{4J^2-1},\tag{37}$$

$$S_0=\sum_{v_0^J}\frac{\langle v_1^J|v_0^J\rangle\langle v_0^J|B(R)|v_1^J\rangle}{E_1^{vJ}-E_0^{vJ}},\tag{38}$$

$$S_1=\sum_{v_0^J}\frac{|\langle v_1^J|v_0^{J+1}\rangle|^2}{E_1^{vJ}-E_0^{vJ+1}},\tag{39}$$

$$S_2=\sum_{v_0^J}\frac{|\langle v_1^J|v_0^{J-1}\rangle|^2}{E_1^{vJ}-E_0^{vJ-1}},\tag{40}$$

$$S_3=\sum_{v_0^J}\frac{\langle v_1^J|v_0^{J-1}\rangle\langle v_0^J|B(R)|v_1^J\rangle}{(E_1^{vJ}-E_0^{vJ-1})(E_0^{vJ}-E_1^{vJ})},\tag{41}$$

$$S_4=\sum_{v_0^J}\frac{\langle v_1^J|v_0^{J+1}\rangle\langle v_0^J|B(R)|v_1^J\rangle}{(E_1^{vJ}-E_0^{vJ+1})(E_0^{vJ}-E_1^{vJ})},\tag{42}$$

and B_v is rotational constant. The diamagnetic term (DMT) takes the form:

$$E_{\mathrm{DMT}}(M^2,B^2)=\langle\Phi_pJM|\hat{\mathbf{H}}_{\mathbf{dm}}|\Phi_pJM\rangle$$
$$=K_{\mathrm{dm}}B^2\left\{h_{00}+\frac{J(J+1)-3M^2}{(2J-1)(2J+3)}\times\left[h_{22}+h_{20}\left(1-\frac{3}{J(J+1)}\right)\right]\right\}.\tag{43}$$

Thus, the closed form of Zeeman energy E_M, given by Eq. (19), in the case of $B1_u^-$ state with fixed v,J,M values can be written as

$$E(B1_u^-,v,J,M)=E_{\mathrm{LPT}}(M,B)+E_{\mathrm{HFT}}(M^2,B^2)+E_{\mathrm{DMT}}(M^2,B^2),\tag{44}$$

where E_{LPT} is linear over M and B, while E_{HFT} and E_{DMT} are quadratic functions of M and B, as defined by the expressions (35)–(43).

In order to determine the $\omega_{MM'}$ values, which govern fluorescence intensities, see Eqs. (9) and (10), let us evaluate the parameters necessary to calculate the energy E_M. The G_z defined by Eq. (29) is the only factor determining the linear LPT term; its numerical value will be taken as $G_z=-1.86$ according to the measurements in Refs. 15 and 25. In signal simulation we will assume $G_{\pm}=2.7=2\eta$ in consistence with the previous data obtained in Refs. 11 and 15. The negative G_z sign for a state with $\Omega=1$ means that we assume that the magnetic moment $\boldsymbol{\mu}_{\mathbf{J}}$ possesses the opposite direction with respect to **J**, the precession angular velocity being equal to $\omega_J=-G_z\mu_BB/[J(J+1)\hbar]$. Rotational constant value $B_{v=2}^{1_u^-}=0.031\,61\ \mathrm{cm}^{-1}$ has been taken from Ref. 14. The S_i values given by Eqs. (38)–(42) were calculated numerically using vibrational wave functions $|v_J\rangle$ obtained by solving Eq. (24) with RKR potentials constructed by means of deperturbed molecular constant sets given in Ref. 15 for $1_u^{\pm}$ and 0_u^+ components of $B\ ^3\Sigma_u^-$ state of $^{130}Te_2$. The results (in $1/\mathrm{cm}^{-1}$) for the $v(J)$ level 2(96) of the 1_u^- state have been obtained, accounting for Eq. (34), as: $S_0=-7.2\times10^{-4}$, $S_1=-1.9\times10^{-2}$, $S_2=-2.9\times10^{-2}$, $S_3=-3.14\times10^{-5}$, $S_4=-2.05\times10^{-5}$. It can be seen from S_i values obtained that the main contribution in the first brackets of Eq. (36) is given by the part of interference term proportional to $G_{\pm}G_zS_0$, namely

$$E_{\mathrm{HFT}}^{\mathrm{int}(S_0)}=\frac{2\eta G_{\pm}G_zS_0}{B_v}\left[\frac{J^2-1}{J^2}\,T(J,M)+\frac{(J^2+1)^2-1}{(J+1)^2}\,T(J+1,M)\right],\tag{45}$$

which is comparable with the terms in the second brackets of Eq. (36), containing S_1 and S_2.

Let us now try to evaluate the electronic parameters h_{00}, h_{20}, and h_{22} of the DMT, see Eq. (43), which are given by Eqs. (31)–(33). In order to obtain crude evaluation of the order of magnitude of h_{00}, we will assume that the $B\ ^3\Sigma_u^-$ complex in Te_2 is of partially Rydberg nature. Then one can estimate the h_{00} value (in a.u.) as $h_{00}=\Sigma_{n=1}^6(n^2/2)[5n^2+1-3l(l+1)]$. Taking into account that the atomic configuration of Te atom is $5s^25p^4$, while in the united atom limit Te_2 approaches the ^{104}Ku configuration $6d^27s^2$, we can estimate the upper limit for h_{00} as being somewhere from 10^4 a.u. to 10^5 a.u. Further, we will assume that, for the Te_2 case considered, as well as for the overwhelming majority of diatomic molecules,[26] the h_{20} and h_{22} values do not exceed several a.u. Using these estimations of electronic parameters h_{00}, h_{20}, and h_{22} and comparing expressions for LPT, HFT, and DMT terms given by Eqs. (35)–(43), it is easy to con-

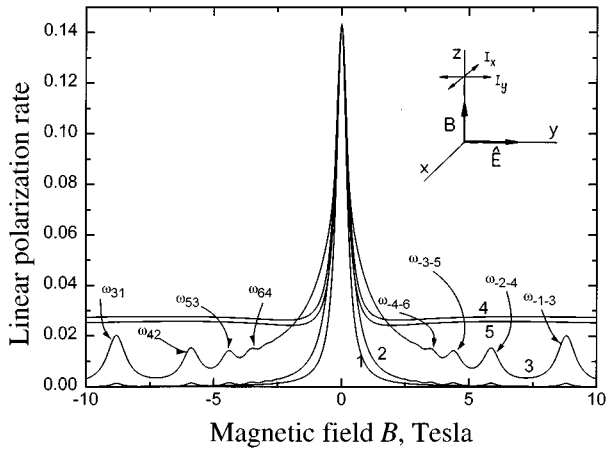

FIG. 3. Calculated magnetic field dependence $P(B)$ of the degree of linear polarization of fluorescence (the geometry is shown in the setting-in). 1—ordinary Lorentz shape Hanle signal in case of linear Zeeman effect term LPT, see Eq. (35); 2—accounting for LPT and for nonlinear Zeeman term HFT, see Eq. (36); 3—accounting for LPT, HFT, homogeneous and heterogeneous magnetic PD; 4—accounting for LPT, heterogeneous and homogeneous magnetic PD; 5—accounting for LPT and heterogeneous magnetic PD. The PD parameters used in calculations are $C_v^{\text{het}} = -6\ \text{s}^{-1/2}$, $\alpha_v^{\text{het}} = 10^4\ \text{s}^{-1/2}\ \text{T}^{-1}$, $C_v^{\text{hom}} = 10^3\ \text{s}^{-1/2}$ and $\alpha_v^{\text{hom}} = 10^3\ \text{s}^{-1/2}\ \text{T}^{-2}$.

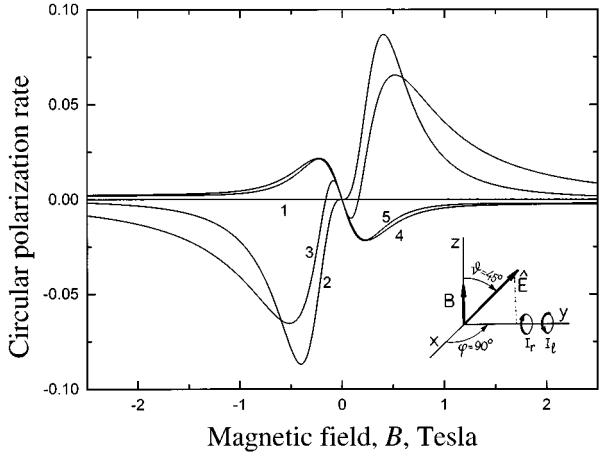

FIG. 4. Calculated magnetic field dependence $C(B)$ of the degree of fluorescence circular polarization, or AOC signal (the geometry is shown in the setting-in). Curves 1–5 are calculated accounting for the same effects as in Fig. 3, respectively.

clude that one can neglect the DMT contribution in the Eq. (44). It is interesting to mention that for low-lying electronic states of diatomic molecules the HFT and DMT values are, as a rule, quite comparable with each other.[26] The latter is caused by the circumstance that, in spite of the fact that diamagnetic constant K_{dm} value in Eq. (13) is approximately 10^4 times smaller than μ_B^2 value in Eq. (12), the large enough energy difference $E_M^{\Phi J} - E_M^{\Phi' J}$ makes the HFT and DMT contributions comparable with each other. As a contrary, in our case of $B\ ^3\Sigma_u^-(\text{Te}_2)$ complex we have $E_M^{|\Omega|=1} - E_M^{\Omega=0}$ equal to ca. 13 cm^{-1} only, which leads to $\mu_B^2/(E_M^{|\Omega|=1} - E_M^{\Omega=0}) \gg K_{\text{dm}}$ and well explains the smallness of the diamagnetic term DMT with respect to HFT.

Let us start with the simulation of a signal appearing in the experimental geometry, which is traditional for Hanle effect manifestation as decrease of fluorescence linear polarization $P(B)=(I_y-I_x)/(I_y+I_x)$ under external magnetic field effect, see Fig. 3. We assume that $\Gamma_{MM'}$ in Eqs. (9) and (10) possesses a constant value $\Gamma_{MM'} \cong \Gamma$, being independent of magnetic field, which means the absence of anisotropic collisions (see discussion in Refs. 4 and 12) and of magnetic PD. In particular, the value $\Gamma = 8.55 \times 10^6\ \text{s}^{-1}$ was used as determined in Refs. 15 and 27. Curve 1 in the figure corresponds to the ''traditional'' Hanle signal of Lorentz shape, which appears in the case of linear Zeeman effect containing LPT only, that is when all B^2-dependent terms are neglected in Eq. (44). Accounting for the HFT in the form given by Eq. (36) produces the signal depicted by curve 2 in Fig. 3, which demonstrates the slightly less steepness if compared with curve 1. Additional maxima of very small amplitude can be distinguished on curve 2 in high B region, that is when the fluorescence is already almost completely depolarized by the linear Zeeman effect. These maxima have apparently to be connected with the crossings of magnetic M sublevels with $|M-M'|=2$ caused by nonlinear Zeeman effect.

We will now proceed to the appearance of the degree of circularity $C(B)$, see Eqs. (7), (9), (10), caused by B^2 terms in E_M, when the condition (4) for $\omega_{MM'}$ is fulfilled. The geometry of excitation and observation of fluorescence is shown in Fig. 4 and is consistent with $\vartheta=45°$, $\varphi=90°$ in Eqs. (9) and (10). Curves 1 and 2 in Fig. 4 are calculated for the same $E_M(B)$ dependencies as discussed above in connection with Fig. 3. Curve 1 in Fig. 4 is strictly zero since linear Zeeman effect is not able to cause AOC.[4,12] Curve 2 demonstrates a pronounced AOC phenomenon caused by quadratic Zeeman effect term HFT given by Eq. (36). It is important to stress that such $C(B)$ signal is an odd function of B, having zero derivative at $B=0$. The last feature can be clearly seen from the Fig. 5, curve 2, which is the same curve depicted in

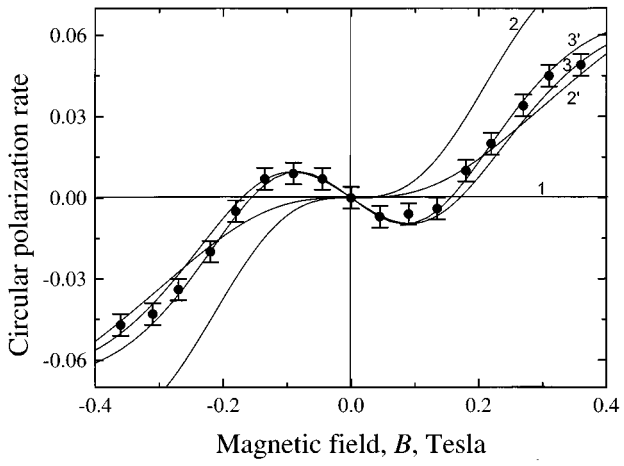

FIG. 5. Fitting of experimentally obtained AOC signal in $C(B)$ at the same geometry as in Fig. 4. Curves 1–3 are the same as in Fig. 4. Curve 2′ ignores the interference term $E_{\text{HFT}}^{\text{int}}$ in quadratic Zeeman effect, see Eq. (36), while curve 3′ differs from curve 3 by ignoring homogeneous PD. The parameters obtained by fitting are: $C_v^{\text{het}} = -6\ \text{s}^{-1/2}$, $\alpha_v^{\text{het}} = 9 \times 10^3\ \text{s}^{-1/2}\ \text{T}^{-1}$, $G_{\pm}=2.7$.

enlarged scale. Curve 2 in Fig. 5 differs markedly from the signal depicted by curve $2'$ in Fig. 5, which was calculated without accounting for $E_{\mathrm{HFT}}^{\mathrm{int}}$ in Eq. (36), as it had taken place in our previous treatment[11] [unfortunately the sign of G_z in formulas (3), (11) and (13) of Ref. 11 is inconsistent with the definition of G_z following from Eqs. (1) and (4) of Ref. 11]. The major difference between curves 2 and $2'$ in Fig. 5 ensures one of the important role of the interference term $E_{\mathrm{HFT}}^{\mathrm{int}}$ appearing because of $B1_u^+ \sim B0_u^+$ wave function mixing by electron–rotation perturbation operator $\hat{\mathbf{V}}$, see Eq. (17). Figure 5 contains also the experimental results (depicted by black circles) taken from Ref. 11. And what is important, the results of the more complete treatment, presented by curve 2, is much farther from describing the experimental points. Moreover, in any choice of fitting parameters (which would lead into contradiction with independently obtained results of Ref. 15), the calculation based on quadratic Zeeman energy shift terms, or on $\omega_{MM'}$ contribution only, are not able to reproduce the additional extrema of experimental $C(B)$ values near $B=\pm 0.1$ T, see Fig. 5.

B. Magnetic PD effect, or $\Gamma_{MM'}$ contribution

Let us now account for $\Gamma_{MM'}$ dependence on magnetic field caused by magnetic field induced PD. We will consider the cases of homogeneous and heterogeneous PD separately, accounting for $1_u^- \sim 1_u^\pm$ and $1_u^- \sim 0_u^-$ interactions respectively, according to the discussion in Sec. IV. Then, adapting again the theory developed in Sec. III, we are able to obtain the explicit formulas for the matrix elements which describe $1_u^- \sim 1_u^\pm$ and $1_u^- \sim 0_u^-$ magnetic PD in Γ_M expression (15). In doing so, for homogeneous PD $1_u^- \sim 1_u^\pm$, one can obtain, by applying Eqs. (18), (29) and Table I, the following expressions for $\hat{\mathbf{H}}_{\mathrm{pm}}$ operator matrix elements with $\Omega=\Omega'$:

$$\langle \Omega JM|\hat{\mathbf{H}}_{\mathbf{pm}}|\Omega JM\rangle = -\frac{\mu_B \mathrm{BMG}_z}{J(J+1)}, \tag{46}$$

$$|\langle \Omega JM|\hat{\mathbf{H}}_{\mathbf{pm}}|\Omega J-1M\rangle|^2 = \mu_B^2 B^2 G_z^2 \frac{J^2-1}{J^2}\, T(J,M), \tag{47}$$

where $T(J,M)$ is given by Eq. (37). Analogously, for heterogeneous PD $1_u^- \sim 0_u^-$, the $\mathbf{H}_{\mathrm{pm}}$ operator matrix elements with $\Omega'=\Omega\pm 1$ can be found, by accounting for Eq. (30), as

$$\langle \Omega JM|\hat{\mathbf{H}}_{\mathbf{pm}}|\Omega' JM\rangle = \frac{\mu_B \mathrm{BMG}_\pm}{\sqrt{J(J+1)}}, \tag{48}$$

whilst the nonzero diamagnetic $\hat{\mathbf{H}}_{\mathrm{dm}}$ operator matrix elements can be found, by applying Eqs. (18), (32) and Table I, as

$$\langle \Omega JM|\hat{\mathbf{H}}_{\mathbf{dm}}|\Omega' JM\rangle = K_{\mathrm{dm}} \frac{B^2 h_{21}}{2} \frac{1}{\sqrt{J(J+1)}} \left[\frac{-J(J+1)+3M^2}{(2J-1)(2J+3)}\right]. \tag{49}$$

Note that for the $1_u^- \sim 0_u^-$ case the interaction matrix elements $\langle \Omega JM|\hat{\mathbf{H}}_{\mathrm{pm}}|\Omega' J\pm 1M\rangle$ disappear.

Putting the expressions obtained into Eq. (15) and taking into account the fact that the rovibronic matrix elements of intramolecular interaction can be described by Eqs. (25)–(27), we arrive at final expressions in explicit form:

$$\Gamma_M^{\mathrm{hom}}(1_u^- \sim 1_u^\pm) \cong 2\pi |\langle v_J|\epsilon_J\rangle|^2 \left[V_{\mathrm{hom}}^2 - \frac{2\mu_B BM V_{\mathrm{hom}} G_z}{J(J+1)} + \frac{\mu_B^2 B^2 G_z^2}{2} \left\{ 1 - \left(\frac{4M^2}{J(J+1)} - \frac{3(4M^2-1)}{(2J-1)(2J+3)} \right) \right\} \right.$$
$$\left. + 2K_{\mathrm{dm}} B^2 V_{\mathrm{hom}} \left\{ h_{00} + \left(h_{22} + h_{20}\left(1 - \frac{3}{J(J+1)} \right) \right) \frac{J(J+1)-3M^2}{(2J-1)(2J+3)} \right\} \right] \equiv C_v^2 - \frac{2BMC_v\alpha_v}{J(J+1)} + \frac{B^2\alpha_v^2}{2} \left[1 \right.$$
$$\left. - \left(\frac{4M^2}{J(J+1)} - \frac{3(4M^2-1)}{(2J-1)(2J+3)} \right) \right] + 2B^2 C_v \left\{ \beta_v^{(0)} + \left[\beta_v^{(1)} + \beta_v^{(2)} \left(1 - \frac{3}{J(J+1)} \right) \right] \frac{J(J+1)-3M^2}{(2J-1)(2J+3)} \right\}, \tag{50}$$

$$\Gamma_M^{\mathrm{het}}(1_u^- \sim 0_u^-) \cong 2\pi \left[\langle v_J|\epsilon_J\rangle \right|^2 \left\{ \frac{2\eta^2 J(J+1)}{(2\mu R_c^2)^2} + \frac{2\mu_B BM\eta G_\pm}{2\mu R_c^2} + \frac{\mu_B^2 B^2 M^2 G_\pm^2}{2J(J+1)} - \frac{K_{\mathrm{dm}} B^2 \eta h_{21}}{2\mu R_c^2} \left(\frac{3M^2 - J(J+1)}{(2J-1)(2J+3)} \right) \right\}$$
$$\equiv 2C_v^2 J(J+1) + 2C_v \alpha_v BM + \frac{\alpha_v^2 B^2 M^2}{2J(J+1)} - \beta_v^{(3)} C_v B^2 \left(\frac{J(J+1)-3M^2}{(2J-1)(2J+3)} \right), \tag{51}$$

where $|\langle v_J|\epsilon_J\rangle|^2$ are the Franck–Condon densities (FCD), R_c is the crossing point of the two potential curves, see Fig. 1, $\beta_v^{(i)}$ are the diamagnetic PD constants, V_{hom} and $\eta \equiv \eta_{\mathrm{het}}$ are the electronic parts of the matrix elements of homogeneous and heterogeneous intramolecular interactions, respectively. It is important that all these parameters are independent of M, B, and J in explicit form. We have passed in the second part of Eqs. (50) and (51) to the following traditional notations: C_v is the natural PD constant,

$$C_v^{\mathrm{hom}} = \sqrt{2\pi}\langle v_J|\epsilon_J\rangle V_{\mathrm{hom}}, \quad C_v^{\mathrm{het}} = \sqrt{2\pi}\langle v_J|\epsilon_J\rangle \frac{\eta}{2\mu R_c^2}, \tag{52}$$

whilst α_v is the constant of paramagnetic PD,

$$\alpha_v^{\rm hom}=\sqrt{2\pi}\langle v_J|\epsilon_J\rangle\mu_B G_z, \quad \alpha_v^{\rm het}=\sqrt{2\pi}\langle v_J|\epsilon_J\rangle\mu_B G_{\pm}. \tag{53}$$

It can be easy seen that the relations obtained are consistent with the general expression given by Eq. (20). From Eqs. (50) and (51) one can also conclude that for $J\gg 1$ the contribution into Γ_M of the term describing interference between natural and magnetic PD, which is proportional to $C_v\alpha_v$ and linear over *BM*, is negligible in the case of homogeneous PD when compared to the case of heterogeneous PD. This can be explained by the presence of the factor $1/[J(J+1)]$ in Eq. (50), as distinct from Eq. (51).

Let us now try to estimate the values of C_v, α_v, and $\beta_v^{(i)}$ parameters in Eqs. (50)–(53) for the case of $B1_u^-$ state PD in Te_2. We will start with FCD $|\langle v_J|\epsilon_J\rangle|^2$ evaluation based on Morse shape approximation of 0_u^- and $1_u^{\pm}$ potential curves responsible for the PD. In doing so, we have used vibrational constant ω_e values given in Ref. 16 for $^3\Pi_u$, $^3\Sigma_u^+$, and $^3\Delta_u$ states. The anharmonic constant $\omega_e x_e$ values were estimated from the knowledge of electronic Te_2 terms for these states, as well as from the $^3P_2+{}^3P_2$ dissociation limit. The equilibrium internuclear distance R_e values for the states under discussion were chosen in the way to provide the condition that intersections of the respective 0_u^- and $1_u^{\pm}$ potential curves with the repulsive branch of the RKR $B1_u^{\pm}$ state potential curve are taking place at reasonable R_c values, namely 2.6 Å $\leqslant R_c < R_e^{B1_u}$ which correspond to the Mulliken's c^--type PD.[23] The energy-normalized vibrational wave functions $|\epsilon_J\rangle$, belonging to continuum spectrum, were calculated by numeric solving of Eq. (24). As a result, the following FCD estimations were obtained: 10^{-4}–10^{-6} l/cm^{-1} for $B1_u^-\sim 0_u^-$ PD and 10^{-6}–10^{-8} l/cm^{-1} for $B1_u^-\sim 1_u^{\pm}$ PD. The $\hbar^2/2\mu R_c^2$ value is of the order of 0.1 cm^{-1}. Since the natural PD rate of the level can not exceed its reciprocal lifetime τ_{vJ}^{-1}, which is given in Table II, one can easy obtain the following estimations of natural PD rates upper limits: $|C_v^{\rm het}|\leqslant 60\ {\rm s}^{-1/2}$ and $C_v^{\rm hom}\leqslant 10^3\ {\rm s}^{-1/2}$. Let us also suppose that the h_{21} values entering Eq. (50) do not exceed 10^2 a.u., while the values of G_z and $G_{\pm}$ are of the order of one a.u. Then we arrive at the following estimations: $\alpha_v^{\rm hom}\cong 10^2$–$10^3\ {\rm s}^{-1/2}\,{\rm T}^{-1}$, $\alpha_v^{\rm het}\cong 10^3$–$10^4\ {\rm s}^{-1/2}\,{\rm T}^{-1}$, $\beta_v^{(0)}\leqslant 10^2\ {\rm s}^{-1/2}\,{\rm T}^{-2}$, $\beta_v^{(1)}\cong\beta_u^{(2)}\leqslant 1\ {\rm s}^{-1/2}\,{\rm T}^{-2}$, $\beta_v^{(3)}\leqslant 10^{-2}\ {\rm s}^{-1/2}\,{\rm T}^{-2}$. Thus, if our electronic parameter estimations are correct, we can well neglect the diamagnetic term contribution into Γ_M, see Eqs. (50) and (51), as it had been done in the case of E_M calculations.

Let us pass to PD signals simulations. Figure 6 demonstrates the circularity signals caused exclusively by PD effect, or by $\Gamma_{MM'}$ contribution. Calculations were performed by using the above estimated values of C_v and α_v for either heterogeneous (curve 1) or homogeneous (curve 2) PD. The calculations are made by putting Eq. (50) or Eq. (51), respectively, into expression (3) for $\Gamma_{MM'}$, which enters Eqs. (8)–(10), under assumption that $\omega_{MM'}$ is independent of M, which means that we neglect B^2 terms in Eq. (44) or, equivalently, we neglect $\omega_{MM'}$ contribution into AOC. As it can be seen, the heterogeneous PD produces a pronounced dispersion type circularity signal, whereas the AOC signal produced by homogeneous PD is almost nonobservable.

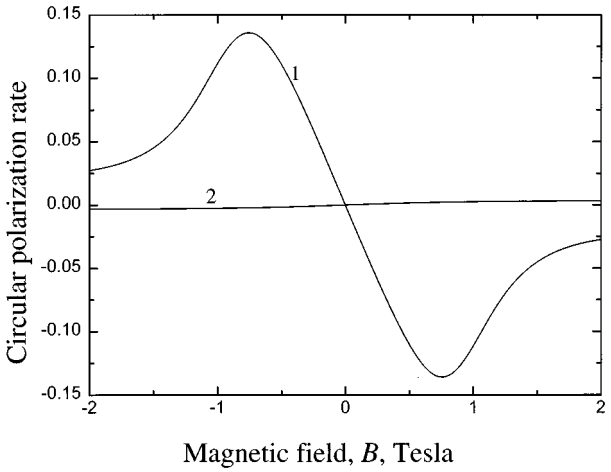

FIG. 6. Comparison of AOC signals in fluorescence circularity $C(B)$ caused by heterogeneous (curve 1) and homogeneous (curve 2) PD, calculated with maximal C_v, α_v values, namely $C_v^{\rm hom}=|C_v^{\rm het}|\sqrt{2J(J+1)}\cong 8.2\times 10^3\ {\rm s}^{-1/2}$, $\alpha_v^{\rm hom}=10^3\ {\rm s}^{-1/2}\,{\rm T}^{-1}$, $C_v^{\rm het}=-60\ {\rm s}^{-1/2}$, $\alpha_v^{\rm het}=10^4\ {\rm s}^{-1/2}\,{\rm T}^{-1}$. Geometry and other parameters are the same as in Figs. 4 and 5.

It is interesting to trace the PD manifestation in wide B range Hanle signals $P(B)$, see Fig. 3. Curves 4 and 5 in Fig. 3 demonstrate the distortion of Lorentz's shape Hanle signal, which is caused by magnetic PD only, that is when the B^2 terms are neglected in $\omega_{MM'}$ calculations. It seams that the remaining nonzero degree of polarization at large B values, see curves 4 and 5, is caused by such $\Gamma_{MM'}$ growing with B which does not change much the $\omega_{MM'}/\Gamma_{MM'}$ ratio. The most interesting is the $P(B)$ behavior in the case when all effects are taken into account, see curve 3 in Fig. 3. As it was checked from the E_M pattern calculation, the pronounced signal broadening in B range of $(1\div 3)$ T, see curve 3, is caused by numerous overlapping nonzero field crossings of magnetic sublevels $M, M\pm 2$ with $96>|M|>6$. Starting from $|B|\geqslant 3$ T, the nonzero field crossings for each particular $|M|\leqslant 6$ value become quite distinguishable, which is understandable for two reasons. First, the absorption–emission cross sections for P-, R-type molecular transitions have maximal values near $M=0$.[12,21] Second, the level crossing peaks for $|M|\leqslant 6$ are much better separated since they occur at largest $|B|$ for the smallest $|M|$ values, see Eq. (19). Of course, such crossings, produced by the influence of quadratic Zeeman energy terms, can be slightly distinguished also on curve 2, see Fig. 3, possessing, however, much smaller amplitude because of fast coherence destruction. It is thus clear that the nonzero magnetic field level crossing signals are pronounced so well in the case depicted by curve 3 due to the ''delay'' in $P(B)$ diminution, which occurs because magnetic PD shows the tendency to increase $\Gamma_{MM'}$ with B growing.

The role of $\Gamma_{MM'}$ contribution in wide B range AOC signals is demonstrated by curves 3–5 in Fig. 4, which are calculated using the same parameters as in the case of analogous curves in Fig. 3. The most interesting is the behavior of curve 3, which is calculated accounting for all effects in

$\omega_{MM'}$ and $\Gamma_{MM'}$ and demonstrates the appearance of additional maxima caused by $\Gamma_{MM'}$ contribution, having opposite signs with respect to the maxima caused by B^2 terms in $\omega_{MM'}$. It can be also seen that the nonzero field level crossings do not manifest themselves in the $C(B)$ signal, as distinct from the $P(B)$ dependence. Curves 4 and 5 are calculated neglecting the HFT contribution in $\omega_{MM'}$. Since curve 4, obtained by accounting for both heterogeneous and homogeneous PD, almost coincides with curve 5, in which only heterogeneous PD was taken into account, the role of homogeneous PD is negligible. This result is in consistence with Fig. 6 and its discussion.

Since the PD-induced AOC leads to opposite sign $C(B)$ signal when compared to the quadratic Zeeman effect, see Fig. 4, it looked promising to fit experimental data, given in Fig. 5, by accounting simultaneously for both nonlinear Zeeman effect and magnetic PD. If one neglects the homogeneous PD effect, it is possible to obtain simultaneously three parameters from $C(B)$ data fitting, namely: the electronic matrix element $G_{\pm}$ of paramagnetic Zeeman Hamiltonian defined by Eq. (30), the rate constant $\alpha_v^{\rm het}$ of paramagnetic heterogeneous PD, and the rate constant $C_v^{\rm het}$ of natural heterogeneous PD. The best fitting was obtained at $G_{\pm}=2.7$, $C_v^{\rm het}=\pm 6\ {\rm s}^{-1/2}$ and $\alpha_v^{\rm het}=\mp 9\times 10^3\ {\rm s}^{-1/2}\ {\rm T}^{-1}$, see curve $3'$ in Fig. 5. It is however impossible to judge about the signs of $C_v^{\rm het}$ and $\alpha_v^{\rm het}$ separately except that their signs have to be opposite. Comparison of curve $3'$ with the curve 3, which was calculated by including into calculation the estimated upper limits of homogeneous PD parameters $C_v^{\rm hom}=10^3\ {\rm s}^{-1/2}$ and $\alpha_v^{\rm hom}=10^3\ {\rm s}^{-1/2}\ {\rm T}^{-1}$, confirms that accounting for $B1_u^-\sim 1_u^{\pm}$ PD practically does not imply the fitting.

VI. DISCUSSION AND CONCLUSIONS

The effect of AOC is an exclusively sensitive tool to investigate the quadratic terms both in Zeeman energy shifts ($\omega_{MM'}$ contribution) and magnetic PD ($\Gamma_{MM'}$ contribution). The above effects produce large enough fluorescence circularity signal $C(B)$ under linear polarized excitation, which disappears completely when the quadratic terms are absent. It should be stressed that the conventional Hanle effect, which is observed via changes of the degree of linear polarization $P(B)$, is almost insensitive to the presence of both quadratic Zeeman energy shift terms and magnetic PD effects in the experimentally applied region of B, as it can be seen from Fig. 7. Indeed, the experimental $P(B)$ data can be equally well described by the simplest Lorentz shape dependence and by the dependence accounting for all abovementioned effects, see curves 1 and 3 in Fig. 7.

Since the influence of $\omega_{MM'}$ and $\Gamma_{MM'}$ produce circularity signals of different sign and shape, see Fig. 4, the $\omega_{MM'}$ and $\Gamma_{MM'}$ contributions can be easy separated, in the processing of $C(B)$ data, at least at certain dynamic parameters of the states under study. The $\omega_{MM'}$ contribution allows, in particular, to determine the electronic matrix element $G_{\pm}$ of magnetic field induced heterogeneous $|\Omega-\Omega'|=1$ interaction which, in its turn, is connected with the electronic matrix element η of electron–rotation Ω, Ω' state mixing, see Eqs.

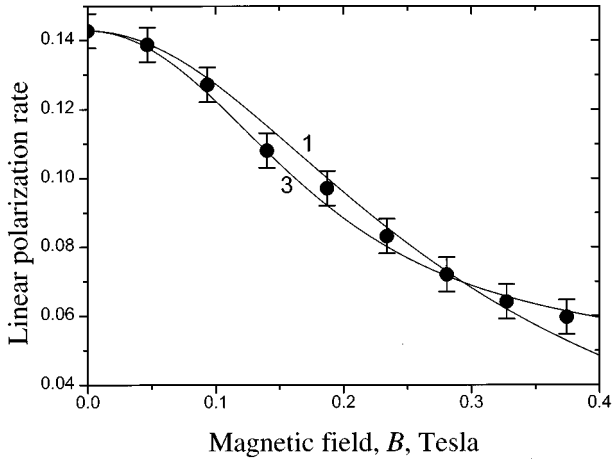

FIG. 7. Fitting of experimentally obtained Hanle signals in degree of linear polarization $P(B)$. Geometry, parameter values and curve numbering are the same as in Fig. 3. 1—Lorentz shape signal; 3—the signal accounting for all effects.

(27) and (30). The $\Gamma_{MM'}$ contribution studies yield new possibilities in investigating PD phenomena. First of all, it is quite surprising that the characteristic additional maxima produced by PD contribution into $C(B)$ signal allow to judge, from the first glance, about the heterogeneous type of PD. And, what is more, it is possible to determine separately, from one fit, both the constant $C_v^{\rm het}$ of natural PD and the constant $\alpha_v^{\rm het}$ of magnetic PD. As it is known from I_2 studies,[8–10] due to the interference term $\alpha_v C_v$ it is possible to determine very weak natural PD rate C_v. Also in the case of $^{130}{\rm Te}_2$ $B1_u^-$ state we obtained $C_v^{\rm het}J(J+1)\cong 6.7\times 10^5\ {\rm s}^{-1}$, which is only about 8% of the full relaxation rate $\Gamma=8.55\times 10^6\ {\rm s}^{-1}$ for $v=2(96)$ level.

As it can be seen from Eqs. (52) and (53), it is possible to use the PD parameters $C_v^{\rm het}=\pm 6\ {\rm s}^{-1/2}$, $\alpha_v^{\rm het}=\mp 9\times 10^3\ {\rm s}^{-1/2}\ {\rm T}^{-1}$, obtained for the $B1_u^-$ state of Te_2, in order to evaluate the ratio of electronic matrix elements $\eta_v^{\rm het}\equiv\eta$ and $G_{\pm}$:

$$\frac{\alpha_v^{\rm het}}{C_v^{\rm het}}\cong\frac{\sqrt{2\pi}\langle v|\epsilon\rangle\mu_B G_{\pm}}{\sqrt{2\pi}\langle v|\epsilon\rangle(\eta/2\mu R_c^2)}=2\mu R_c^2\mu_B\frac{G_{\pm}}{\eta}. \tag{54}$$

Using the evaluated $\hbar^2/(2\mu R_c^2)\cong 0.1\ {\rm cm}^{-1}$ value and taking $\mu_B=0.467\ {\rm cm}^{-1}\ {\rm T}^{-1}$, one obtains, by applying Eqs. (27) and (30), the following $G_{\pm}/\eta$ value:

$$\frac{G_{\pm}}{\eta}=\frac{g_l J_{a\pm}+(g_s-g_l)S_{\pm}}{J_{a\pm}}$$
$$\cong 1+\frac{S_{\pm}}{J_{a\pm}}\cong\frac{\alpha_v^{\rm het}}{C_v^{\rm het}2\mu R_c^2\mu_B}\cong -3.2\times 10^2. \tag{55}$$

The fact that $G_{\pm}/\eta$ ratio is so large means that almost complete cancellation of $L_{\pm}$ and $S_{\pm}$ takes place. Indeed, since $\hat{\mathbf{J}}_{\mathbf{a}\pm}=\hat{\mathbf{L}}_{\pm}+\hat{\mathbf{S}}_{\pm}$, Eq. (55) yields $L_{\pm}\cong -1.0031 S_{\pm}$. Hence, for $B1_u^-$ state of Te_2 the values of electronic matrix elements $L_{\pm}$ and $S_{\pm}$ almost coincide, being opposite in signs. This

striking point was observed also for the $B\ ^3\Pi_{0_u^+}$ state of I_2 molecule,[10] where the ratio $L_{\pm} \cong -1.0435 S_{\pm}$ was obtained.

Let us try to trace how the results of PD studies by magnetic AOC are consistent with other data about dynamic characteristics of $B1_u^-$ state in Te_2 molecule. An interesting possibility to obtain some indirect information about PD based on global deperturbation analysis (GDA) was considered in Ref. 15. In particular, the experimentally measured[28] transition moment dependence on internuclear distance R allowed us to evaluate the ''pure'' spontaneous lifetime values $\tau_{\rm sp}^{\rm est}$ of the level, see the last column of Table II. From comparison of these values with the effective lifetimes $\tau_{\rm sp}^{\rm exp}$ of Table II which were directly measured,[27] one can arrive at the following conclusions. First, as it can be seen from the table, $\tau_{\rm sp}^{\rm exp}$ exhibits faster decrease with v for the $B1_u^-$ component than for the $B1_u^+$ one, which allows one to suppose the existence of an additional channel for the $B1_u^-$ state decay. Second, the $B1_u$ rovibronic $v(J)$ level energies practically coincide for $v=8(70)$ and $5(131)$ states, being equal to 1315.66 and 1313.58 cm^{-1}, respectively. Then, if only homogeneous c^--type PD, which is J independent, would take place, one had to expect almost equal PD rates for both levels. However, as it can be seen from Table II, $\tau_{8(70)}^{\rm exp} \ll \tau_{5(131)}^{\rm exp}$. If one supposes that the heterogeneous $B1_u^{\pm}$ state PD takes place via $B1_u^+ \sim 2_u^+$ interaction, then the PD rate for the 5(131) level had to be ca. 131/70 times larger then the one for the 8(70) level, which also disagrees with experimental data. Hence, the only PD mechanism, which is consistent with $\tau_{v(J)}^{\rm exp}$ measurements, is that only the $B1_u^-$ state predissociates heterogeneously, whereas the $B1_u^+$ state does not. And this is possible only if $B1_u^- \sim 0_u^-$ PD takes place, which is in complete consistence with the data obtained from magnetic AOC studies, see Sec. V.

It is worth to mention that only the simplest PD mechanism, namely the direct predissociation, was considered in the present investigation. In the situation of quite dense state pattern, which is the case for Te_2 molecule, one cannot exclude the influence of indirect (or accidental) PD,[19] which takes place via an intermediate state. Due to this fact, as well as because of the restricted amount of experimental data, we do not pretend our analysis of PD mechanisms in $(B1_u^-)Te_2$ to be complete. Nevertheless, the general features of AOC phenomenon, caused by simultaneous effect of magnetic field induced energy shift and changes in PD rate, which were revealed in the present work, will not change with elaboration of PD mechanisms. It is worth to mention that the nonlinear terms both in E_M and in Γ_M magnetic field dependencies occur also under more precise, nonperturbative treatment, which has to be applied at large B values.

ACKNOWLEDGMENTS

The authors are indebted to Professor Jacque Vigue for stimulating exchange with information, to Dr. Elena Pazyuk and Dr. Ilze Klincare for useful discussions, as well as to Olga Nikolayeva for technical assistance. Support from ISF Grant No. LF 7000 and from Joint ISF and Latvian Government Grant LJ 7100 is gratefully acknowledged. Three of us (M.A., M.T., and R.F.) are grateful for the support from Latvian Science Council (Grant No. 93.256), as well as for the support from European Commission in the frame of PECO Human Capital & Mobility (Networks) program, Contract No. ERBCIPDCT940633. One of us (A.V.S.) is grateful for the support from Russian Foundation for Basic Research (Grant No. 93-03-18059).

[1] U. Fano, Phys. Rev. **133**, B828 (1964).
[2] V. N. Rebane, Opt. Spectrosc. (USSR) **24**, 163 (1968).
[3] M. Lombardi, C. R. Acad. Sci. Ser. B **265 B**, 191 (1967).
[4] M. P. Auzinsh, and R. S. Ferber, J. Chem. Phys. **99**, 5742 (1993).
[5] X. L. Han, and G. W. Schinn, Phys. Rev. A **43**, 266 (1991).
[6] R. C. Hilborn, L. R. Hunter, K. Johnson, S. K. Peck, A. Spencer, and J. Watson, Phys. Rev. A **50**, 2467 (1994).
[7] H. Avci, and H.-P. Neitzke, J. Phys. B **22**, 495 (1989).
[8] M. Broyer, J. Vigue, and J. C. Lehmann, Chem. Phys. Lett. **22**, 313 (1973).
[9] J. Vigue, M. Broyer, and J. C. Lehmann, J. Phys. B **7**, L158 (1974).
[10] J. Vigue, M. Broyer, and J. C. Lehmann, J. Phys. **42**, 937, 949, 961 (1981).
[11] I. P. Klincare, M. Ya. Tamanis, A. V. Stolyarov, M. P. Auzinsh, and R. S. Ferber, J. Chem. Phys. **99**, 5748 (1993).
[12] M. Auzinsh and R. Ferber, *Optical Polarization of Molecules* (Cambridge University, Cambridge, 1995).
[13] M. P. Auzinsh and R. S. Ferber, Phys. Rev. Lett. **69**, 3463 (1992).
[14] J. Verges, C. Effantin, O. Babaky, J. d'Incan, S. J. Prosser, and R. F. Barrow, Phys. Scr. **25**, 338 (1982).
[15] E. A. Pazyuk, A. V. Stolyarov, M. Ya. Tamanis, and R. F. Ferber, J. Chem. Phys. **99**, 7873 (1993).
[16] K. Balasubramanian, and Ch. Ravimohan, J. Mol. Spectrosc. **126**, 220 (1987).
[17] C. Cohen-Tannoudji, Ann. Phys. (Paris) **7**, 423, 469 (1962).
[18] L. P. Landau and E. M. Lifshitz, *Quantum Mechanics* (Pergamon, London, 1965).
[19] H. Lefebvre-Brion and R. W. Field, *Perturbation in the Spectra of Diatomic Molecules* (Academic, New York, 1986).
[20] J. H. van Vleck, Rev. Mod. Phys. **23**, 213 (1951).
[21] R. N. Zare, *Angular Momentum* (Wiley, New York, 1988).
[22] A. R. Edmonds, *Angular Momentum in Quantum Mechanics* (Princeton U.P., Princeton, 1974).
[23] R. S. Mulliken, J. Chem. Phys. **33**, 247 (1960).
[24] G. Herzberg, *Molecular Spectra and Molecular Structure. I. Spectra of Diatomic Molecules* (Van Nostrand, Princeton, NJ 1957).
[25] I. P. Klintsare, M. Ya. Tamanis, and R. S. Ferber, Opt. Spectrosc. (USSR) **67**, 720 (1989).
[26] M. Mizushima, *Theory of Rotating Diatomic Molecules* (Wiley, New York, 1975).
[27] I. P. Klincare and M. Ya. Tamanis, Chem. Phys. Lett. **180**, 63 (1991).
[28] R. S. Ferber, Ya. A. Harya, and A. V. Stolyarov, J. Quant. Spectrosc. Radiat. Transfer **42**, 143 (1992).